

Towards quantitative accuracy in first-principles transport calculations: The GW method applied to alkane/gold junctions

M. Strange and K. S. Thygesen

*Center for Atomic-scale Materials Design, Department of Physics
Technical University of Denmark, DK - 2800 Kgs. Lyngby, Denmark*

(Dated: November 21, 2021)

The calculation of electronic conductance of nano-scale junctions from first principles is a long standing problem in molecular electronics. Here we demonstrate excellent agreement with experiments for the transport properties of the gold/alkanediamine benchmark system when electron-electron interactions are described using the many-body GW approximation. The main difference from standard density functional theory (DFT) calculations is a significant reduction of the contact conductance, G_c , due an improved alignment of the molecular energy levels with the metal Fermi energy. The molecular orbitals involved in the tunneling process comprise states delocalized over the carbon backbone and states localized on the amine end groups. We find that dynamical screening effects renormalize the two types of states in qualitatively different ways when the molecule is inserted in the junction. Consequently, the GW transport results cannot be mimicked by DFT calculations employing a simple scissors operator.

I. INTRODUCTION

The conductance of a molecule sandwiched between metallic electrodes is sensitive to the chemical and electronic structure of the molecule as well as the detailed atomic structure of the metal-molecule contact. Variations in the contact geometry beyond experimental control lead to an undesired spread in measured conductance properties. For the most commonly used thiol anchoring group, these effects are rather pronounced due to the many possible contact geometries resulting from the large strength of the Au-S interaction. Amine groups have been shown to produce more well defined transport properties¹ which can be understood from the relatively weak Au-NH₂ bond leading to larger structural selectivity².

Even for a given junction geometry, a quantitatively accurate description of electron transport from first principles remains a formidable task. Numerous studies based on density functional theory (DFT) have shown a significant overestimation of conductance relative to experimental values³⁻¹⁴ (an exception to this trend occurs for small molecules, like H₂^{15,16} and CO^{17,18}, which chemisorp strongly to the electrodes resulting in resonant transport through broad, partially filled resonances). The inability of DFT to describe off-resonant tunneling in the simplest molecular junctions limits the predictive power of the DFT-based approach to qualitative trends. It is now broadly accepted that the failure of DFT is mainly due to its wrong description of the molecular energy levels. Indeed, physically motivated correction schemes have shown that much improved agreement with experiments can be obtained after shifting the DFT molecular energy levels^{13,14}. Such corrections are supposed to remove the self-interaction errors inherent in standard DFT exchange-correlation (xc) functions and account for image charge effects induced by the metal contacts. The drawback of the approach is that it assumes a weak coupling between molecular orbitals and

metal states and treats the image plane position as a free parameter.

The (self-consistent) GW approximation¹⁹, which is rooted in many-body perturbation theory, was recently found to yield a considerable improvement over DFT for the conductance of gold/benzenediamine junctions²⁰. Physically, the GW approximation corresponds to Hartree-Fock theory with the bare Coulomb interaction $v = 1/|\mathbf{r} - \mathbf{r}'|$ replaced by a dynamically screened Coulomb interaction $W(\omega) = \epsilon^{-1}(\omega)v$. In contrast to standard DFT, the GW approximation is self-interaction free and includes image charge effects due to the metal contacts through the correlation part of the self-energy²¹⁻²³. As a consequence, it provides quantitatively accurate predictions of energy gaps in systems with highly diverse screening properties ranging from isolated molecules^{24,25} over semiconductors²⁶, to metals²⁷. This property becomes particularly important for a metal-molecule interface where the electronic structure changes from insulating to metallic over a few Angstrom.

In this work we use the GW approximation to study the role of exchange-correlation effects for the energy level alignment and electron transport in short alkane chains coupled to gold electrodes via amine linker groups. The gold/alkane junction is a benchmark system for molecular charge transport and have been exhaustively investigated experimentally^{1,12,28-39}. We focus here on the amine-linked alkanes to avoid the uncertainties related to the gold-thiol contact geometry which is presently under debate⁴⁰⁻⁴⁵. We note that very recently it was shown that alkanes can be bound directly to gold electrodes without the use of anchoring groups⁴⁶.

The transport mechanism in (short) saturated molecular wires is coherent tunneling via molecular orbitals with energy far from the Fermi energy. The conductance versus chain length (N) thus follows an exponential law of the form

$$G = G_c \exp(-\beta N) \quad (1)$$

Recent experimentally reported values for the decay constant β of alkanediamine/gold junctions are in the range 0.9-1.0 per C atom^{1,12,31}, but earlier measurements also showed values around 0.8³⁰. Although previous studies based on DFT have yielded β values within the experimental range, the contact conductance, G_c , is typically overestimated by around an order of magnitude³⁻¹⁰. By comparing DFT and GW calculations for N -alkanediamine molecules with $N = 2, 4, 6$ we show that the wrong G_c values are a result of incorrect level alignment in the DFT calculations. Indeed, GW yields a G_c in close agreement with experimental values. We find a pronounced orbital and length dependence of the quasiparticle (QP) corrections to the DFT energies resulting from the different shape and localization of the molecular orbitals. The QP corrections range from -0.5 to -2.5 eV and can be qualitatively explained from a classical image charge model.

II. METHOD

The junction geometries were optimized using the real space projector augmented wave method GPAW^{47,48} with a grid spacing of 0.2 Å and the PBE functional for exchange and correlation (xc)⁴⁹. The molecules were attached to Au(111) surfaces, modeled by an eight layer thick 4×4 slab via small four atom tips as shown in Figure 1. The surface Brillouin zone was sampled on a 4×4 Monkhorst pack k -point grid, and the structures including molecule, Au tips, and outermost Au surface layers were relaxed until the residual force was below 0.03 eV/Å. We have considered N -alkanediamine junctions with $N = 2, 4$ and 6. Key structural parameters can be found here⁵⁰. For calculations of the molecules in the gas-phase we include 16 Å of vacuum between molecules in repeated super cells.

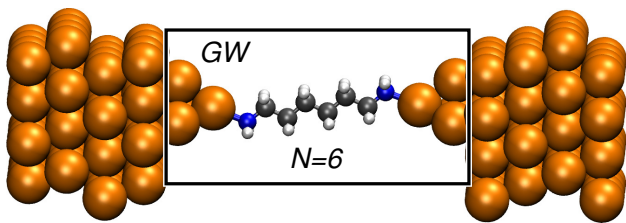


FIG. 1: Supercell used to model the gold/alkanediamine junctions. Similar supercells have been used for $N = 2$ and 4 (not shown) and key structural parameters can be found here⁵⁰. The black box indicates the extended molecule region within which the GW self-energy is evaluated. The inclusion of the Au tips in the extended molecule is sufficient to include screening effects from the electrodes on the molecular energy levels.

All transport calculations were performed using the method described in detail in Ref.²⁰. In brief we employ a basis set of numerical atomic orbitals corresponding to double-zeta plus polarization (DZP) for the Au atoms

and double-zeta (DZ) for the atoms of the molecules. We use rather diffuse basis functions with a confinement energy shift of 0.01 eV. This ensures that the calculated work function of Au(111) and the Kohn-Sham energy levels of the molecular junction are within 0.1 eV of those obtained from accurate grid calculations²⁰. The transmission function is obtained from the Meir-Wingreen transmission formula^{51,52}

$$T(\varepsilon) = \text{Tr}[G^r(\varepsilon)\Gamma_L(\varepsilon)G^a(\varepsilon)\Gamma_R(\varepsilon)]. \quad (2)$$

The retarded Green function of the extended molecule is calculated from

$$G^r(E) = [(E + i\eta)S - H_0 + V_{xc} - \Delta V_H[G] - \Sigma_L(E) - \Sigma_R(E) - \Sigma_{xc}[G](E)]^{-1} \quad (3)$$

Here S , H_0 , and V_{xc} are the overlap matrix, Kohn-Sham Hamiltonian and the local xc-potential in the atomic orbital basis, respectively. η is a positive infinitesimal.

The lead self-energy, $\Sigma_{L/R}$, incorporates the coupling to the left and right electrodes and is obtained using standard techniques⁵³. The term ΔV_H gives the change in the Hartree potential relative to the DFT Hartree potential already contained in H_0 . Finally, the last term is the many-body xc self-energy which in this work is either the bare exchange potential, V_x , corresponding to Hartree-Fock or the GW self-energy. As indicated both the Hartree potential and the xc self-energy depend on the Green function. The latter is evaluated fully self-consistently using a simple linear mixing of the Green functions. The GW self-energy is evaluated for the extended molecule (indicated by the box in Figure 1). However, only the part corresponding to the molecule is used while the remaining part is replaced by the DFT xc-potential. This is done to include non-local correlation (image charge) effects from the electrodes in the GW self-energy of the molecule while preserving a consistent description of all metal atoms at the DFT level. We have verified that the calculations are converged with respect to the size of the extended molecules, see Ref.²⁰ for more details. We represent all energy dependent quantities in Equation (3) on a large energy grid ranging from -200 eV to 200 eV with an energy grid spacing of 0.01 eV.

III. RESULTS AND DISCUSSION

A. Energy level alignment

The alignment of the molecular energy levels relative to the electrode Fermi level is of great importance for the transport properties of molecular junctions and seems to be the dominating effect at low bias voltage. At higher bias voltages many body calculations on small model systems suggest that electron correlations induce additional shifting and broadening of the molecular levels which can also affect the transport properties⁵⁴. Here we focus on

TABLE I: Calculated HOMO and HOMO-2 energies aligned to the vacuum level and in units of eV.

Method	Orbital	$N = 2$	$N = 4$	$N = 6$
DFT-PBE	HOMO	-4.9	-5.1	-5.1
	HOMO-2	-8.5	-8.2	-8.0
HF	HOMO	-10.2	-10.5	-10.5
	HOMO-2	-13.3	-12.9	-12.8
GW	HOMO	-8.5	-8.6	-8.6
	HOMO-2	-12.2	-11.8	-11.6

TABLE II: Calculated HOMO and HOMO-2 energies in the junction relative to the electrode Fermi level.

Method	Orbital	$N = 2$	$N = 4$	$N = 6$
DFT-PBE	HOMO	-4.3	-4.2	-4.4
	HOMO-2	-6.5	-5.9	-5.7
HF	HOMO	-8.1	-8.1	-8.3
	HOMO-2	-10.4	-9.9	-9.7
GW	HOMO	-4.8	-4.9	-5.2
	HOMO-2	-8.4	-8.2	-8.2

the low bias regime and postpone the finite bias effects to a later study.

The molecular orbitals (MOs) of the alkanediamine chains comprise states which are delocalized over the carbon backbone and states which are localized on the NH_2 end group. We shall consider the highest occupied molecular orbital (HOMO) and HOMO-2 as representatives for the two classes of states, see Figure 2(a). We note that the HOMO-1 is similar to the HOMO with slightly lower energy given by the coupling of the two end groups across the wire. In Table I and II we list the energy of the HOMO and HOMO-2 calculated with DFT-PBE, Hartree-Fock (HF), and GW for the molecules in the gas-phase and junction, respectively. In the gas-phase, all three methods predict the HOMO energy to be almost independent of molecular length. This is clearly due to its end group localized character. In contrast, the energy of the HOMO-2 level shifts upward in energy as the molecular length increases. This reflects its extended nature and can be interpreted as a band discretization effect. To the best of our knowledge no experimental results exists for the ionization potential of alkanediamine molecules. However, for the closely related butane molecule ($N = 2$ alkane with CH_3 end groups) we obtain a GW calculated HOMO energy of -11.4 eV in very good agreement with the experimental ionization potential of 11.2 eV⁵⁵. In comparison, the DFT-PBE HOMO energy is severely underestimated at -7.9 eV. This finding agrees well with previous studies on a larger range of small molecules^{20,24,25}.

In the junction, the molecular orbitals, $|\psi_n\rangle$, have been obtained by diagonalizing the DFT Hamiltonian corresponding to the molecule. The projected density of states

(PDOS) of such a state is then given by the spectral function, $-1/\pi\text{Im}\langle\psi_n|G^r(E)|\psi_n\rangle$, where G is the appropriate Green function (calculated with DFT, HF, or GW). The level position is defined as the first moment of the PDOS. Figure 2(b) shows the PDOS for the HOMO and HOMO-2 for the 6-alkanediamine junction as calculated with DFT-PBE (upper panel) and GW (middle panel). The lower panel shows the PDOS obtained from a DFT calculation where the molecular levels have been shifted to match the GW levels, i.e. after adding to the Kohn-Sham Hamiltonian a generalized scissors operator of the form, $\Sigma_{\text{GSO}}^{\text{DFT}} = \sum_n(\varepsilon_n^{\text{QP}} - \varepsilon_n^{\text{DFT}})|\psi_n\rangle\langle\psi_n|$. Here $\varepsilon_n^{\text{QP}}$ denote the QP energy obtained from the GW calculation. We see that the main features of the GW spectral function can be well reproduced by the shifted DFT Hamiltonian although small differences remain. A similar conclusion was reached in Ref.²⁰ for a gold/benzenediamine junction. The molecular orbital energies from a GW calculation include the dynamical response of the electron system to an added or removed electron through the correlation part of the self-energy. In general correlations tend to shift the filled levels up and the empty levels down relative to the bare Hartree-Fock energies. This is because the inclusion of screening reduces the energy cost of removing/adding electrons to the molecule. When a molecule is brought into contact with a metallic junction its environment changes from insulating to metallic. This implies extra screening of an added or removed electron which will cause the filled levels to shift upwards and the empty levels to shift downwards even more than for the isolated molecules, i.e the gap will shrink relative to its gas-phase value. It has been shown previously that DFT in (semi)local approximations and Hartree-Fock completely misses this important effect²¹⁻²³.

In Figure 2(c) and (d) we show the QP corrections to the HF and DFT Kohn-Sham energy levels as function of molecular length. The results for the HOMO and the HOMO-2 are denoted by circles and squares. We first notice that the QP corrections are very significant with absolute values reaching almost 4 eV with a pronounced orbital and length dependence. The Hartree-Fock QP corrections are all positive showing that HF places the occupied levels lower than predicted by GW. This is in contrast to the corrections to the DFT levels which are all negative in agreement with the well known underestimation of ionization potentials by DFT. In contrast to Hartree-Fock the Kohn-Sham QP corrections are smaller for molecules in the junction rather than in the gas-phase. In fact the DFT HOMO level position is relatively close the GW level position and only lie 0.5-0.8 eV higher. The fact that the DFT-PBE description of molecular energy levels is much better in the junction than in the gas-phase agrees with previous findings^{20,22,56}, and can be explained from the origin of the PBE functional in the homogenous electron gas⁵⁷.

It is instructive to consider the shift in the molecular energy levels due to correlation effects coming from the metal electrodes. In simple terms this corresponds to the

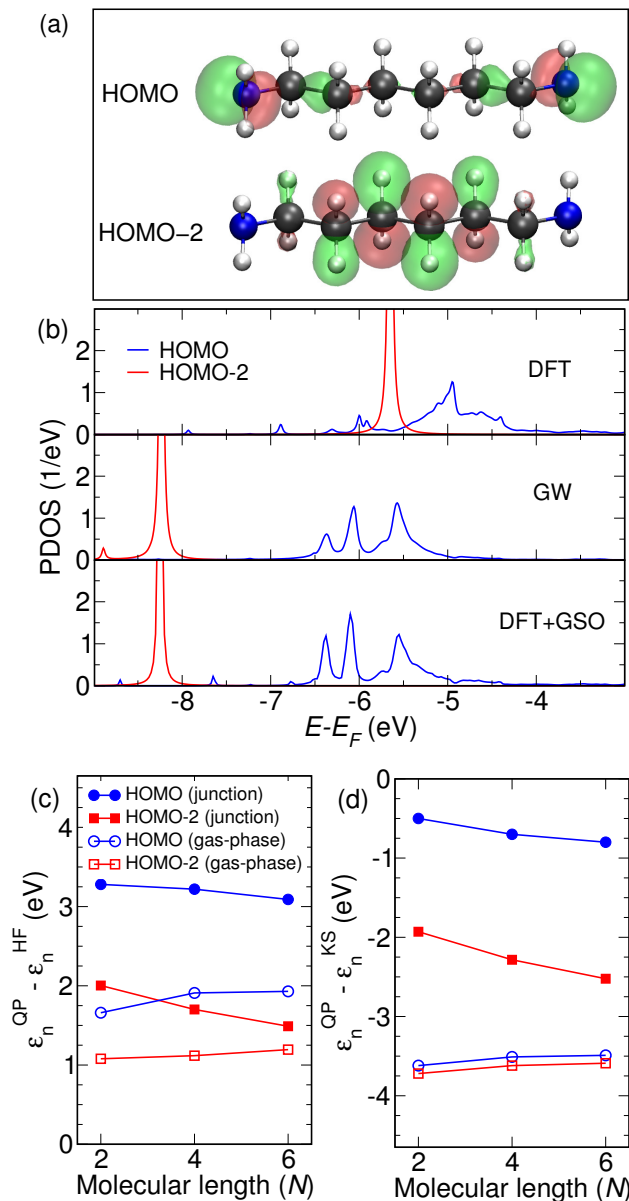


FIG. 2: (a) Isosurfaces for the HOMO and HOMO-2 orbitals of the 6-alkanediamine molecule. (b) HOMO and HOMO-2 PDOS in the junction obtained from DFT-PBE (top), GW (middle) and DFT with a generalized scissor operator (bottom). (c) Quasiparticle corrections to the Hartree-Fock levels in the gas-phase (open symbols) and in the junction (filled symbols) as a function of molecular length N . The HOMO and HOMO-2 are denoted by circles and squares, respectively. (d) Same as (c) but for DFT rather than Hartree-Fock.

shift induced by image charge effects. In order to isolate the part of the correlation energy originating from the metallic electrodes we define the quantity,

$$\Delta\epsilon_{\text{corr},n} = (\epsilon_n^{\text{QP}} - \epsilon_n^{\text{HF}})_{\text{junction}} - (\epsilon_n^{\text{QP}} - \epsilon_n^{\text{HF}})_{\text{gas-phase}} \quad (4)$$

which is shown in Figure 3. The result can be understood qualitatively by considering a classical model to account for the screening effect of the electrodes. Clas-

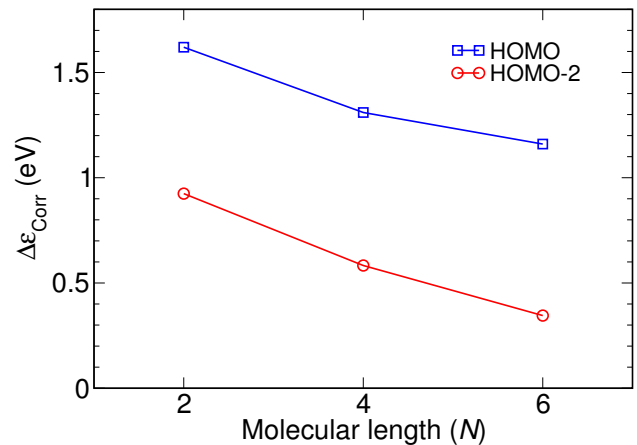


FIG. 3: Change in the correlation energy of the HOMO and HOMO-2 energy levels when the molecules are taken from the gas-phase into the junction. This value represents the shift of molecular levels due to the enhanced screening provided by the metallic electrodes (an image charge effect in simple terms).

sically a charge distribution between two perfect metals will experience an image potential. For example, the image potential for a point charge halfway between two metal surfaces separated by a distance L is $\approx 10.0/L$ (eV \AA)⁵⁸. This predicts a $\propto 1/L$ dependence for the image charge effect. The Au tip atoms in our simulations are about 8 \AA apart for the 2-alkanediamine junction giving a rough estimate of 1.3 eV for the image charge effect in qualitative agreement with the GW calculations. The HOMO experiences a larger image charge effect than the HOMO-2 which can be understood from the fact that its charge density is located closer to the metallic surfaces. In the limit of an infinitely long wire the HOMO-2 will be spread out over the entire molecule and the image charge effect should vanish. On the other hand in this limit the HOMO will stay localized near the surface and therefore approach a non-zero constant image charge potential. If we model the HOMO charge density as a point charge of half an electron on each of the amine groups we can estimate this limiting constant to be $3.6/(2d)$ (eV \AA), where d is the distance to the nearest metal surface. Taking d to be around the Au-N bond length (2.34 \AA) gives a limiting value estimate of 0.8 eV. Again, this seems to be in qualitative agreement with our GW findings.

Finally, we discuss the coverage dependence of the energy level position for alkanediamine-Au junctions. It was shown in Ref.⁵⁹ that the DFT level position for amine linked molecules is strongly dependent on coverage. In contrast to the screening (image charge) effects discussed above, which appear in the correlation part of the self-energy, this is a purely electrostatic effect resulting from the localized surface dipoles formed at the Au-NH₂ bond. To investigate the dependence of the energy levels on coverage for our junctions we have performed DFT calculations for a range of transverse supercell dimensions for

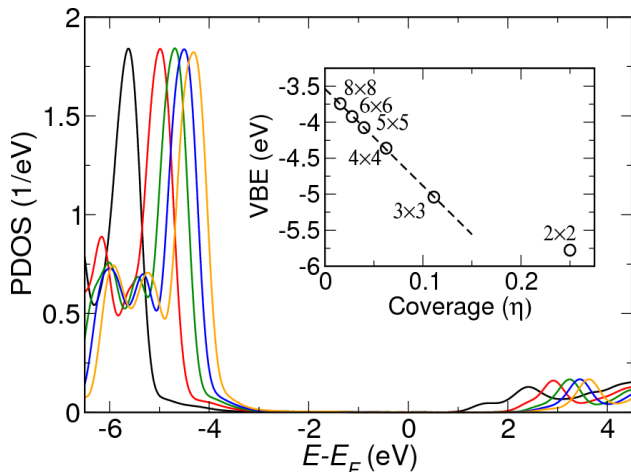


FIG. 4: The molecular valence band edge (or HOMO) as a function of coverage for an $N = 6$ alkane. The numbers indicate the number of surface atoms.

the geometry shown in Figure 1. In Figure 4 we show the PDOS of a methylene unit in the central part of the molecule for transverse super cells with 2×2 to 8×8 surface atoms. The PDOS peaks and band edge is shifting up in energy as the transverse supercell size is increased in agreement with the results of Ref.⁵⁹. The inset shows the energy shift obtained from reading off the shift in the PDOS as a function of coverage defined as $\eta = 1/N_{\text{surface}}$, where N_{surface} is the number of surface atoms. For a supercell dimension of size 3×3 and larger, the shift is seen to be directly proportional with the coverage as expected for a two dimensional array of dipoles⁶⁰. This allow us to extract the electrostatic shift corresponding to the single molecule limit. We find that the electrostatic energy shift when going from a 4×4 supercell to the single molecule limit is indeed significant with a value around 1 eV.

B. Transport calculations

The transmission function of the 2, 4 -and 6-alkanediamine junction geometries were calculated using the GW and the PBE xc potential as approximations for Σ_{xc} in Eq. (3). To include the coverage dependence we have simulated the low coverage limit $\eta = 0^+$ by performing calculations using the 4×4 junction (corresponding to $\eta = 1/16$) with all molecular levels shifted up by 1 eV using a simple scissors operator self-energy.

The transmission function calculated using GW is shown in Figure 5 on a logarithmic scale. The transmission functions for different molecular lengths have very similar shapes in the important region near the Fermi level E_F , however, the magnitude is increasingly suppressed as function of molecular length. The similarity of the transmission functions may at first seem surprising since we have shown that the position of the molecular

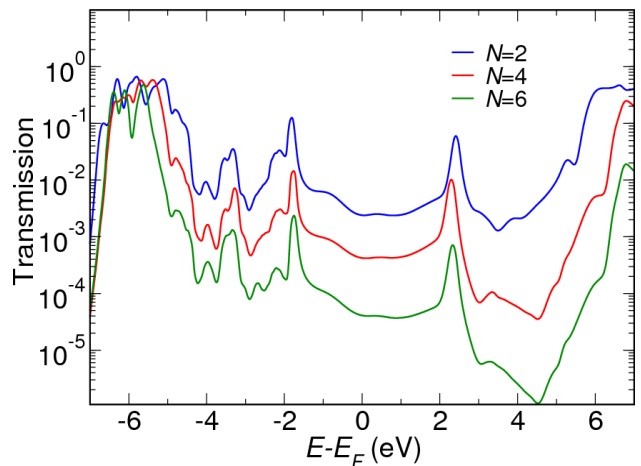


FIG. 5: The transmission function calculated using GW for a molecular length of $N=2, 4$ and 6 .

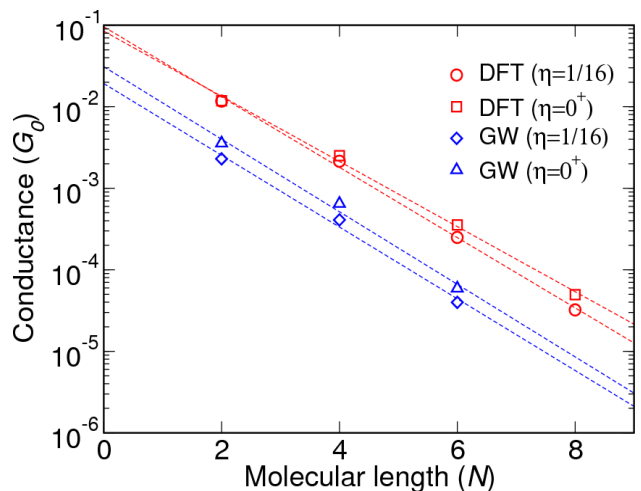


FIG. 6: Calculated conductance plotted as a function of the molecular length for coverages corresponding to 4×4 Au atoms per molecule ($\eta = 1/16$) and extrapolated to the single-molecule limit ($\eta = 0$).

energy levels show some length dependence. In particular the HOMO level was found to decrease in energy by 0.5 eV when N increases from 2 to 6 (see Table II). This shift is indeed visible in transmission function in the range -4.0 to -6.0 eV where the HOMO is located. On the other hand the features in the transmission function around the Fermi level are determined by the local electronic structure of the Au tips .

The zero bias conductance is obtained from the transmission function at the Fermi level, $G = G_0 T(E_F)$ where $G_0 = 2e^2/h$ is the unit of quantum conductance. The zero bias conductance is plotted in Figure 6 as function of molecular length. We have also included the DFT results for comparison. The dashed lines show the best fits to the exponential form $G_N = G_c \exp(-\beta N)$. The values for β and G_c corresponding to the single-molecule limit ($\eta = 0$) and 4×4 Au atoms per molecule ($\eta = 1/16$)

	DFT		GW		Exp.
η	1/16	0	1/16	0	–
G_C	0.11	0.10	0.02	0.04	0.02 ^a , 0.035 ^c
β	0.99	0.92	1.01	1.02	0.97 ^a , 0.93 ^b , 0.91 ^c

^aRef.¹²^bRef.³¹^cRef.¹

TABLE III: Calculated contact conductance G_C in units of G_0 and exponential decay constant β per carbon atom. η denotes the coverage.

are reported in Table III together with experimental values. The rather weak effect of coverage on the conduction properties is in agreement with the findings in Ref.⁶¹ where a 4-alkanediamine Au junction with 3×3 and 4×4 surfaces was considered. Our DFT results are in reasonable agreement with previous DFT studies showing decay factors in the range 0.83 – 1.01 and conductance resistances in the range $(0.09 - 0.28)G_0^{8-10}$. While the β values obtained with GW are rather close to the DFT calculated ones, the contact conductance is reduced by a factor of 3 – 5 depending on the coverage. This is a direct result of the molecular levels lying further away from E_F (by 0.5-2.5 eV, see Figure 2(d)) in GW compared to DFT.

IV. CONCLUSION

We have unraveled the important role of exchange-

correlation effects for the energy level alignment and low-bias conductance of gold/alkanediamine molecular junctions. Based on many-body GW calculations we found that the origin of the overestimation of the contact conductance, G_c , by standard DFT is due to wrong energy level alignment in the junction. The absence of self-interaction and the inclusion of image charge screening effect through the GW self-energy improves the description of the energy levels and yield values for G_c and the decay constant β in good agreement with experiments. The quasiparticle corrections to the DFT energy levels showed a significant orbital dependence ranging from -0.5 eV to -2.5 eV due to the different shape and localization of the molecular orbitals. Our results demonstrate that quantitatively accurate calculations of conductance from first-principles are feasible, although computationally demanding.

V. ACKNOWLEDGMENTS

The authors acknowledge support from the Lundbeck Foundation's Center for Atomic-scale Materials Design (CAMD) and The Danish Center for Scientific Computing.

-
- ¹ L. Venkataraman, J. Klare, I. Tam, C. Nuckolls, M. Hybertsen, and M. Steigerwald, *Nano Lett.* **6**, 458 (2006).
² I. S. Kristensen, D. J. Mowbray, K. S. Thygesen, and K. W. Jacobsen, *J. of Phys.: Condens. Matter* **20**, 374101 (2008).
³ J. Tomfohr and O. Sankey, *Phys. Rev. B* **65**, 245105 (2002).
⁴ A. Sen and C.-C. Kaun, *ACS Nano* **4**, 6404 (2010).
⁵ C. Kaun and H. Guo, *Nano Lett.* **3**, 1521 (2003).
⁶ K. Muller, *Phys. Rev. B* **73**, 045403 (2006).
⁷ M. Paulsson, C. Krag, T. Frederiksen, and M. Brandbyge, *Nano Lett.* **9**, 117 (2009).
⁸ S. Wohlthat, F. Pauly, and J. R. Reimers, *Chem. Phys. Lett.* **454**, 284 (2008).
⁹ S. McDermott, C. B. George, G. Fagas, J. C. Greer, and M. A. Ratner, *J. Phys. Chem. C* **113**, 744 (2009).
¹⁰ W. Sheng, Z. Y. Li, Z. Y. Ning, Z. H. Zhang, Z. Q. Yang, and H. Guo, *J. Chem. Phys.* **131**, 244712 (2009).
¹¹ C. Li, I. Pobelov, T. Wandlowski, A. Bagrets, A. Arnold, and F. Evers, *J. Am. Chem. Soc.* **130**, 318 (2008).
¹² M. S. Hybertsen, L. Venkataraman, J. E. Klare, A. CWhalley, M. L. Steigerwald, and C. Nuckolls, *J. Phys.:Condens. Matter* **20**, 374115 (2008).
¹³ S. Y. Quek, L. Venkataraman, H. J. Choi, S. G. Louie, M. S. Hybertsen, and J. B. Neaton, *Nano Lett.* **7**, 3477 (2007).
¹⁴ D. J. Mowbray, G. Jones, and K. S. Thygesen, *J. Chem. Phys.* **128**, 111103 (2008).
¹⁵ R. Smit, Y. Noat, C. Untiedt, N. Lang, M. van Hemert, and J. van Ruitenbeek, *Nature (London)* **419**, 906 (2002).
¹⁶ D. Djukic, K. S. Thygesen, C. Untiedt, R. Smit, K. Jacobsen, and J. van Ruitenbeek, *Phys. Rev. B* **71**, 161402 (2005).
¹⁷ C. Untiedt, D. Dekker, D. Djukic, and J. van Ruitenbeek, *Phys. Rev. B* **69**, 081401 (2004).
¹⁸ M. Strange, K. S. Thygesen, and K. W. Jacobsen, *Phys. Rev. B* **73**, 125424 (2006).
¹⁹ L. Hedin, *Phys. Rev.* **139**, A796 (1965).
²⁰ M. Strange, C. Rostgaard, H. Hakkinen, and K. S. Thygesen, *Phys. Rev. B* **83**, 115108 (2011).
²¹ J. B. Neaton, M. S. Hybertsen, and S. G. Louie, *Phys. Rev. Lett.* **97**, 216405 (2006).
²² J. M. Garcia-Lastra, C. Rostgaard, A. Rubio, and K. S. Thygesen, *Phys. Rev. B* **80**, 245427 (2009).
²³ K. S. Thygesen and A. Rubio, *Phys. Rev. Lett.* **102**, 046802 (2009).
²⁴ C. Rostgaard, K. W. Jacobsen, and K. S. Thygesen, *Phys. Rev. B* **81**, 085103 (2010).
²⁵ X. Blase, C. Attacalite, and V. Olevano, *Phys. Rev. B* **83**, 115103 (2011).

- ²⁶ M. Hybertsen and S. Louie, Phys. Rev. B **34**, 5390 (1986).
- ²⁷ B. Holm and U. von Barth, Phys. Rev. B **57**, 2108 (1998).
- ²⁸ B. Xu and N. Tao, Science **301**, 1221 (2003).
- ²⁹ V. Engelkes, J. Beebe, and C. Frisbie, J. Am. Chem. Soc. **126**, 14287 (2004).
- ³⁰ F. Chen, X. Li, J. Hihath, Z. Huang, and N. Tao, J. Am. Chem. Soc. **128**, 15874 (2006).
- ³¹ Y. S. Park, A. C. Whalley, M. Kamenetska, M. L. Steigerwald, M. S. Hybertsen, C. Nuckolls, and L. Venkataraman, J. Am. Chem. Soc. **129**, 15768 (2007).
- ³² Z. Huang, F. Chen, P. A. Bennett, and N. Tao, J. Am. Chem. Soc. **129**, 13225 (2007).
- ³³ J. R. Widawsky, M. Kamenetska, J. Klare, C. Nuckolls, M. L. Steigerwald, M. S. Hybertsen, and L. Venkataraman, Nanotechnology **20**, 434009 (2009).
- ³⁴ M. Kamenetska, M. koentopp, A. C. Whalley, Y. S. Park, M. L. Steigerwald, C. Nuckolls, M. S. Hybertsen, and L. Venkataraman, Phys. Rev. Lett. **102**, 126803 (2009).
- ³⁵ H. Song, T. Lee, N.-J. Choi, and H. Lee, Appl. Phys. Lett. **91**, 253116 (2007).
- ³⁶ Y. Kim, T. J. Hellmuth, M. Buerkle, F. Pauly, and E. Scheer, ACS Nano **5**, 4104 (2011).
- ³⁷ C. A. Martin, D. Ding, H. S. J. van der Zant, and J. M. van Ruitenbeek, New J. Phys. **10**, 065008 (2008).
- ³⁸ R. J. Nichols, W. Haiss, S. J. Higgins, E. Leary, S. Martin, and D. Bethell, Phys. Chem. Chem. Phys. **12**, 2801 (2010).
- ³⁹ W. Haiss, S. Martin, L. E. Scullion, L. Bouffier, S. J. Higgins, and R. J. Nichols, Phys. Chem. Chem. Phys. **11**, 10831 (2009).
- ⁴⁰ A. Cossaro, R. Mazzarello, R. Rousseau, L. Casalis, A. Verdini, A. Kohlmeyer, L. Floreano, S. Scandolo, A. Morgante, M. L. Klein, et al., Science **321**, 943 (2008).
- ⁴¹ Y. Wang, Q. Chi, N. S. Hush, J. R. Reimers, J. Zhang, and J. Ulstrup, J. Phys. Chem. C **113**, 19601 (2009).
- ⁴² O. Voznyy, J. J. Dubowski, J. Yates, J. T., and P. Maksymovych, J. Am. Chem. Soc. **131**, 12989 (2009).
- ⁴³ P. D. Jadzinsky, G. Calero, C. J. Ackerson, D. A. Bushnell, and R. D. Kornberg, Science **318**, 430 (2007).
- ⁴⁴ M. Walter, J. Akola, O. Lopez-Acevedo, P. D. Jadzinsky, G. Calero, C. J. Ackerson, R. L. Whetten, H. Groenbeck, and H. Hakkinen, Proc. Natl. Acad. Sci. (USA) **105**, 9157 (2008).
- ⁴⁵ M. Strange, O. Lopez-Acevedo, and H. Hakkinen, J. Phys. Chem. Lett. **1**, 1528 (2010).
- ⁴⁶ Z. L. Cheng, R. Skouta, H. Vazquez, J. R. Widawsky, S. Schneebeli, W. Chen, M. S. Hybertsen, R. Breslow, and L. Venkataraman, Nature Nanotechnology **6**, 353 (2011).
- ⁴⁷ J. Enkovaara, C. Rostgaard, J. J. Mortensen, J. Chen, M. Dulak, L. Ferrighi, J. Gavnholt, C. Glinsvad, V. Haikola, H. A. Hansen, et al., J. Phys.:Condens. Matter **22**, 253202 (2010).
- ⁴⁸ A. H. Larsen, M. Vanin, J. J. Mortensen, K. S. Thygesen, and K. W. Jacobsen, Phys. Rev. B **80**, 195112 (2009).
- ⁴⁹ J. Perdew, K. Burke, and M. Ernzerhof, Phys. Rev. Lett. **77**, 3865 (1996).
- ⁵⁰ (We use the equilibrium PBE lattice constant of 4.18 Å for Au. The distance between the second outermost Au(111) atomic surface layers in the left and right electrode was fixed at 21.59 Å, 24.10 Å and 26.63 Å for the $N=2$, 4 and 6 junction, respectively. The resulting relaxed N-Au bond length are 2.34 Å, 2.35 Å and 2.33 Å).
- ⁵¹ Y. Meir and N. S. Wingree, Phys. Rev. Lett. **68**, 2512 (1992).
- ⁵² K. S. Thygesen, Phys. Rev. B **73**, 035309 (2006).
- ⁵³ K. S. Thygesen and K. W. Jacobsen, Chem. Phys. **319**, 111 (2005).
- ⁵⁴ K. S. Thygesen, Physical Review Letters **100**, 166804 (2008).
- ⁵⁵ URL <http://webbook.nist.gov/cgi/cbook.cgi?ID=C106978&Units=SI&Mask=20#Ion-Energetics>.
- ⁵⁶ M. Dell'Angela, G. Kladnik, A. Cossaro, A. Verdini, M. Kamenetska, I. Tamblyn, S. Y. Quek, J. B. Neaton, D. Cvetko, A. Morgante, et al., Nano Lett. **10**, 2470 (2010).
- ⁵⁷ M. Rohlfing, Phys. Rev. B **82**, 205127 (2010).
- ⁵⁸ C. J. Chen, *Introduction to Scanning Microscopy* (Oxford University Press, 1993).
- ⁵⁹ J.-g. Wang, E. Prodan, R. Car, and A. Selloni, Phys. Rev. B **77**, 245443 (2008).
- ⁶⁰ A. Natan, L. Kronik, H. Haick, and R. T. Tung, Adv. Mater. **19**, 4103 (2007).
- ⁶¹ X. Y. Feng, Z. Li, and J. Yang, J. Phys. Chem. C **113**, 21911 (2009).